Title:

Changes in distribution, morphology and ultrastructure of chloride cell in Atlantic salmon during an AGD infection

Short running title: impact of amoebic gill disease on chloride cells

Yao-Chung Chang[1], Harry Hamlin-Wright[1], Sean Monaghan[1], Tharangani Herath[2], Johanna Baily[1], Jorge del Pozo[3], Jamie Downes[4], Andrew Preston[1], Lynn Chalmers[1], Nilantha Jayasuriya[5], James E. Bron[1], Alexandra Adams[1] and Sophie Fridman[1]

[1] Institute of Aquaculture, School of Natural Sciences, University of Stirling, Stirling, Stirlingshire, Scotland, FK9 4LA

[2] Department of Animal Production, Welfare and Veterinary Sciences, Harper Adams University, Newport, Shropshire, England, TF10 8NB

[3] The Royal (Dick) School of Veterinary Studies, Easter Bush Campus, Midlothian, Scotland, EH25 9RG

[4] Marine Institute, Fish Health Unit, Rinville, Oranmore, Co. Galway, Ireland, H91 R673

[5] School of Veterinary Sciences, University of Bristol, England, BS40 5DU

Acknowledgements

The authors would like to thank Dr William Roy and Mr Chessor Matthews at the Machrihanish Marine Environmental Research Laboratory (MERL) for their invaluable advice and help with planning and conducting the AGD cohabitation challenge and sampling. The TEM imaging

was performed at the Electron Microscopy Lab., University of Edinburgh – with special thanks to Mr Steven Mitchell for his excellent technical skill in sample preparation and assistance with imaging. The authors would also like to thank Ms. Debbie Faichney for her technical advice and support with histology. This study has received funding from the European Union's Horizon 2020 research and innovation programme under Grant Agreement no. 634429 (ParaFishControl). This output reflects only the author's view and the European Union cannot be held responsible for any use that may be made of the information contained herein. Biotechnology and Biological Sciences Research Council grant award reference: BB/M028224/1.

Conflict of Interest

No potential conflict of interest of all authors is reported.

Abstract

Amoebic gill disease (AGD) is emerging as one of the most significant health challenges affecting farmed Atlantic salmon in the marine environment. It is caused by the amphizoic amoeba *Neoparamoeba perurans*, with infestation of gills causing severe hyperplastic lesions, compromising overall gill integrity and function. This study used histology, transmission electron microscopy (TEM), immunohistochemistry and transcript expression to relate AGD-associated pathological changes to changes in the morphology and distribution of chloride cells (CCs) in the gills of Atlantic salmon (*Salmo salar* L.) showing the progression of an AGD infection. A marked reduction in numbers of immunolabeled CCs were detected and a changing pattern in distribution and morphology was closely linked with the level of basal epithelial hyperplasia in the gill. In addition, acute degenerative ultrastructural changes to CCs at the lesion site were observed with TEM. These findings were supported by the early onset down-regulation of Na^+/K^+-ATPase transcript expression. This study provides supportive evidence that histological AGD lesion assessment was a good qualitative tool for AGD scoring and corresponded well with qPCR genomic *P. perurans* quantification. Ultrastructural changes induced in salmon CCs as a result of AGD are reported here for the first time.

Keywords: *Neoparamoeba perurans*, mitochondria rich cell, Na^+/K^+-ATPase, ionoregulatory cells, salmonid, transmission electron microscopy.

Introduction

Amoebic gill disease (AGD) is one of the most significant health challenges affecting farmed Atlantic salmon (*Salmo salar* L.) in the marine environment (Adams, Crosbie, & Nowak, 2012) First reported in farmed salmon stocks in Tasmania in the mid 1980s (Munday, 1986), it has since been found in most Atlantic salmon producing regions worldwide *i.e*. France (Findlay & Munday, 1998), Ireland (Rodger & McArdle, 1996), Spain (Rodger & McArdle, 1996), Chile (Bustos, Young, Rozas, Bohle, Ildefonse, Morrison, & Nowak, 2011), Norway (Steinum, Kvellestad, Rønneberg, Nilsen, Asheim, Fjell, Nygard, Olsen, & Dale, , 2008), Faroe Islands (Oldham, Rodger, & Nowak, 2016) and South Africa (Mouton, Crosbie, Cadoret, & Nowak, 2014). Of further concern in Norway, AGD has now been described in the cleaner fish species used to delouse farmed Atlantic salmon infected with sea lice *Lepeophtheirus salmonis*, including Ballan wrasse *Labrus bergylta* (Karlsbakk,Olsen, Einen, Mo, Fiksdal, Aase, Karkgraff, Skar, & Hansen, 2013) and lumpfish *Cyclopterus lumpus* (Haugland, Olsen, Rønneseth, & Andersen, 2017). In Scotland, AGD has been an emerging and serious problem since 2006 and is associated with major economic losses due to a reduction in growth, increased mortality and related treatment expenses (Rodger, 2014; Shinn, Pratoomyot, Bron, Paladini, Brooker, & Brooker, 2015). It was estimated that AGD-related mortality losses cost around £10 million GBP in 2006 in Norway and £60 million GBP in 2011 in Scotland (Shinn et al., 2015).

The aetiological agent of AGD is *Neoparamoeba perurans*, a cosmopolitan, free-living marine amphizoic amoeba (Young, Crosbie, Adams, Nowak, & Morrison, 2007). Amoebae attach to the gills causing white raised lesions, usually beginning at the base of the filaments and spreading along the gill arch (Nowak, 2012). I nfected gills often covered with abundant mucus secretion when observed during routine gill examination

(Nowak & Munday, 1994; Rodger & McArdle, 1996; Taylor, Kube, Muller, & Elliott, 2009; Nowak, 2012). The pathological sequence of AGD infection is well documented (Zilberg & Munday 2000; Nowak & Munday 1994; Adams and Nowak 2001; Adams and Nowak 2003; Morrison, Cooper, Koop, Rise, Bridle, Adams, & Nowak, 2006; Young, Cooper, Nowak, Koop, & Morrison, 2008) and has been characterised as 'a focal fortification strategy of the host tissue concurrent with a migration of immunoregulatory cells to lesion-affected areas' (Adams & Nowak, 2003). Other clinical signs include lethargy, respiratory distress and an increased rate of opercular movement (Munday, Zilberg, & Findlay, 2001). The severity and progression of the disease are routinely monitored and scored according to the gill scoring system described by Taylor, Muller, Cook, Kube & Elliott (2009) in which macroscopic pathology of the gills is described on a scale of clear (0) to heavy (5).

Chloride cells (CCs) (also known as mitochondria-rich cells or ionocytes) are highly specialised cells that are present on the afferent edge of the filamental epithelium of the gill, in particular in the interlamellar region (Perry, 1997; Van Der Heijden, Van Der Meij, Flik, & Wendelaar Bonga, 1999; Wilson & Laurent, 2002). Changes in the distribution dynamics of chloride cells have been described during the progression of AGD infections (Adams & Nowak, 2001; Adams & Nowak, 2003; Roubal, Lester & Foster, 1989; Munday, Forster, Roubal, & Lester, 1990; Nowak & Munday, 1994). Immunohistochemical identification of chloride cells, using anti-Na^+/K^+-ATPase, shows the sloughing of chloride cells from a forming lesion and fewer CCs found in association with larger lesions (Adams & Nowak, 2001) with a concomitant reduction in Na^+/K^+-ATPase positive chloride cells in association with larger advanced stage lesions similarly

reported (Adams & Nowak, 2001; Adams & Nowak, 2003; Roubal, Lester & Foster, 1989; Munday, Forster, Roubal, & Lester, 1990; Nowak & Munday, 1994).

The aim of this study was to expand the current knowledge concerning the histopathological and specifically ultrastructural characteristics of lesions associated with the early stagechanges occurring in an AGD infection and, in particular, its impact on the integrity and distribution of gill chloride cells (CCs). The aims of the study were thus to (1) examine histological changes of gills during the early stages of AGD infection (*i.e.* gill score of less than two) (2) measure gill Na^+/K^+-ATPase transcript expression and (3) relate these findings to morphological, ultrastructural and distributional changes of CCs as a response to early stage AGD in Atlantic salmon. The study predominantly focused on evaluation of experimental data collected from fish showing early signs of AGD infection (*i.e.* gill score of less than two), with comparative analysis also conducted using archival histological materials from Atlantic salmon with high gill score for infection with AGD (*i.e.* gill score of four and above).

Materials and methods

Experimental fish

All sampling in the present study was carried out at the Marine Environmental Research Laboratory (MERL), Institute of Aquaculture, Machrihanish, Scotland, UK, 55.4 N 5.7 W).

A group of stock fish that had arrived from a freshwater facility to the current sea water facilities in September 2015 were held in a 13000 L tank. The facility is supplied with flow-

through sea-water (35 ppt) filtered at 100 µm. All fish were maintained under ambient temperature (min.: 11 °C, max.: 13 °C) and fed with commercial salmon pellets equivalent to 1% of their body weight per day. These fish had been freshwater treated against AGD two weeks prior to initiation of the experiment and had scored 0 for AGD afterwards, based on the gill scoring system according to Taylor Muller, Cook, Kube, & Elliott, (2009).

Laboratory challenge of AGD was induced in Atlantic salmon using the cohabitation method developed at the Institute of Aquaculture. Challenge cohabitants or 'seeders' were produced using a stock of fish infected with AGD as part of an ongoing *in vivo* amoebae challenge. Forty post-smolts were randomly selected from the above group of stock fish and were cohabited in a 1-m-diameter tank (400 L) with 20 infected 'seeder' fish (mean gill score of 1.5 ± 0.5), which had been previously ventrally panjet marked (Alcian blue, 0.065g mL^{-1}, Sigma-Aldrich, UK) in order to allow their differentiation within the group. The level of AGD infection within the challenged group was monitored weekly; fish were anaesthetised using tricaine methanesulfonate (MS-222) at 75 mg/L and gross gill scores recorded, as described above. Clinical signs of AGD were detected in challenged fish at 4 weeks post-exposure *i.e.* gross gill score range; 0-1.5, based on the scoring system according to Taylor Muller, Cook, Kube, & Elliott, (2009) and the sampling process was immediately initiated. This was carried out in May 2016.

Fish husbandry, welfare and experimental protocols were conducted according to UK Home Office requirements under the Animals (Scientific Procedures) Act 1986.

Fish sampling

A total of 15 fish were randomly sampled from amongst the challenged group; fish (weight range 0.67 – 1.08 kg; fork length range 37.4 – 50 cm), euthanised by anaesthetic overdose (MS-222) followed by destruction of the brain (Schedule 1 method: 4.2 of the Home Office

guidelines). In addition a further five fish were randomly sampled from amongst the stock group of non-experimentally challenged fish (weight range 0.41 – 0.65 kg; fork length range 32.7 – 37.1 cm) as above. Gross gill scores were recorded from all sampled fish, as described above and, based on these observed scores, four infection level categories (Clear (A), Very Light (B), Light (C) Very Mild (D)) were designated to enable the different grades of early stage AGD (*i.e.* gross gill score range; 0-1.5; Table 1) to be distinguished.

In addition, wax embedded gill tissues, obtained from a previous 4-week AGD cohabitation challenge conducted in April 2014 at the same research facility, was used (Chalmers, Taylor, Roy, Preston, Migaud, & Adams, 2017). Fish had been sampled at week 4 post-challenge when fish were displaying gross gill scores of 3.5-4.5 and were grouped within the infection level category; Heavy (E) (Table 1).

Histology

For histological analysis of samples taken in 2016, the entire third left gill arch was excised, rinsed briefly in seawater and fixed in 10% neutral buffered formalin until processing and embedding in paraffin wax. Gill samples from the previous challenge experiment in 2014 had been taken from the second left gill arch, fixed in 4% paraformaldehyde for 24 h at 20 °C then transferred to 70% ethanol prior to processing and embedding. All tissues were then sectioned at 5 μm, stained with haematoxylin and eosin, screened microscopically using an Olympus CX31 microscope (Olympus Life Science Solutions, Southend-on-Sea, UK) and then digitised in high resolution for further analysis using an Axio Scan.Z1 slide scanner (ZEISS, Cambridge, UK).

Semi-quantitative lesion assessment

From the histological examination, histological changes of gills were evaluated and grouped into 3 categories: 1/ Small Focal, 2/ Medium Focal and 3/ Locally Extensive. Five filaments showing visible signs of AGD infection were selected from three individual fish within each infective category (Group A, B, C, D & E; Table 1). The total number of lesions visible amongst the five filaments were counted and grouped into the respective lesion categories. A filament was only counted when the central venous sinus was visible along two-thirds of the filament length and secondary lamellae were the same length bilaterally till the tip of the filament (Speare, Arsenault, MacNair, & Powell, 1997).

Immunohistochemistry

A portion of gill containing a visible lesion (consisting of 10-15 filaments) from the second left gill arch was removed, rinsed in seawater and fixed in 4% paraformaldehyde for 24 h at 20 °C. It was then transferred to 70% ethanol and stored at -20°C for immunohistochemical analysis (IHC). A monoclonal antibody (MAb) against Na^+/K^+-ATPase (IgGα5), used to specifically label chloride cells, was obtained from the Developmental Studies Hybridoma Bank, Department of Biological Sciences, University of Iowa, Iowa, USA.

Samples were processed, embedded in paraffin wax and then sectioned. Sections were de-waxed by placing the slides in successive xylene baths (2 x 5 min) and gradually rehydrated through graded alcohol baths. The targeted tissues on the sections were encircled with wax by using PAP pen (ImmEdge^{TM} pen, Vector Labs, California, UK) to keep reagents localised on the tissue preparations. To inhibit endogenous peroxidase activity and block non-specific binding sites, sections were incubated in 3% (v/v) hydrogen peroxide in methanol for 10 min at 20^{o}C, washed in the PBS (3 x 3 min) and then incubated with 10% normal goat serum for 30 min at 20^{o}C. Primary antibody (anti-Na^+/K^+-ATPase; Mab, IgGα5), diluted 1:200, was

added for 1 h at 20°C and the sections were washed with PBS (3 x 3 min). The sections were then incubated with goat anti-mouse IgG MAb conjugated to horseradish peroxidase (HRP) (1:100, A4416, Sigma, USA) for 1 h at 20°C. Sections were then washed in tap water (3 x 10 min) and bound antibody peroxidase was labelled by using ImmPACT DAB Peroxidase (HRP) Substrate (SK-4105; Vector Laboratories, USA) according to the manufacturer's instructions. Sections were counterstained with Mayer's haematoxylin for 4 min, washed thoroughly with tap water and gradually dehydrated (70% ethanol for 3 min, 100% ethanol for 5 min and 2 successive xylene baths (5 min each)), Slides were then coverslipped using Pertex^{TM} before being examined under an Olympus CX31 light microscope (Olympus Life Science Solutions, Southend-on-Sea, UK), and digitised in high resolution for further analysis using an Axio Scan.Z1 slide scanner (ZEISS, Cambridge, UK).

Negative control IgG isotype-matched MAbs were included in each IHC run and included sections incubated with mouse monoclonal IgG Anti-Green fluorescent protein (GFP) antibodies (1:500, Roche, Germany). Secondary antibody negative controls included sections incubated in PBS instead of MAbs.

Transmission electron microscopy (TEM)

For ultrastructural examination, a 4-5 filament wide portion of gill from the second left gill arch containing a visible lesion was taken from three fish from Group D (Infection level category; very mild) and a similar sized portion of gill from the second left gill arch was taken from three fish from Group A (Infection level category; clear). Samples were fixed in 3% glutaraldehyde for 3 h, washed in PBS (3 x 10 min) and stored at 4^{o}C. Samples were then washed in 0.1 M sodium cacodylate buffer (3 x 10 min), post-fixed in 1% osmium tetroxide in 0.1 M sodium cacodylate (45 min) and finally washed in 0.1 M sodium cacodylate buffer (3 x

10 min). Samples were dehydrated in a series of graded ethanol (50, 70, 90 and 100%) in propylene oxide (2 x 10 min) and embedded in TAAB 812 resin (TAAB Laboratories Equipment, Berkshire, UK). Sections were cut at 60 nm and subsequently stained using uranyl acetate and lead citrate for contrast then examined under JEOL JEM-1400 Plus transmission electron microscope (JEOL, USA). Digital images were collected from a GATAN one view camera (GATAN, USA).

Molecular analyses

For molecular analyses, small pieces of gill (4-5 filaments) were taken from sites with a visible lesion (L) and no visible lesion (N) from the second left gill arch and immediately preserved either in 1 mL 90% ethanol and stored at -20 ^{o}C or 1 mL RNAlater® (Thermo Fisher Scientific) and stored at -70 ^{o}C for qPCR verification and quantification of *P. perurans* and down-stream gene expression analysis of Na^{+}/K^{+}-ATPase, respectively. For Group A (clear) two pieces of apparently uninfected tissue were taken randomly.

Real time qPCR

DNA extraction

Total DNA was extracted from gills (100 mg) which had been previously fixed in 90% ethanol. DNA was extracted using the QiAamp tissue mini kit® (Qiagen) according to the manufacturer's protocol for purification from animal tissues. The quality and quantity of extracted DNA was checked and measured by NanoDrop (Nanodrop 1000, Thermo Fisher Scientific, UK) and all DNA samples were standardised to the concentration of 50 nMol μL^{-1} and stored at -20 °C.

Genomic qPCR for *P. perurans* detection and quantitation

The extracted DNA samples were used for quantification and confirmation of the presence of

P. perurans by real-time qPCR at the Marine Institute in Galway, Ireland according to Downes, Henshilwood, Collins, Ryan, O'Connor, Rodger, MacCarthy & Ruane (2015). The *N. perurans* loading obtained from Groups A-E were statistically compared using non-parametric Kruskal-Wallis test following an Anderson-Darling test for normality using Minitab® 17 software (Minitab Ltd, Coventry, UK)). For *post-hoc* testing, the Mann-Whitney U test (Minitab® 17 software (Minitab Ltd, Coventry, UK)) was used.

RNA Extraction

Total RNA was extracted from gills (approximately 100 mg) that had previously been stored in RNAlater, using the TRIzol® extraction technique (Thermo Scientific, UK) according to manufacturer's instructions with modifications. Briefly, the samples were incubated with TRIzol® on ice for 30 min before homogenising with 5 metal beads (BioSpec Products, UK) using a Mini-Beadbeater (Mini-Beadbeater-16, BioSpec Products, USA) for 60 sec. Following organic solvent extraction with TRIZol, RNA was precipitated in 200 μL RNA precipitation solution (1.2M NaCl, 0.8 M Sodium Citrate Sesquihydrate (Sigma Aldrich, UK)) combined with 200 μL isopropanol (Sigma Aldrich, USA) then incubated at 20 °C for 10 min prior to centrifugation at 20,000 x *g* for 10 min at 4 °C. The RNA pellet was washed in 1 mL of 75 % ethanol and left to air dry for 5 min at 20 °C. RNA was then dissolved in 50 μL of RNAse free water (Thermo Scientific, UK) on ice before measuring RNA quality and quantity by NanoDrop (Nanodrop 1000, Thermo Scientific). RNA samples were diluted to a concentration range of 300 and 600 ng μL^{-1} before storing at -70 °C until RT-qPCR analysis was performed at Harper Adams University, UK.

Complementary DNA (cDNA) synthesis

First strand cDNA synthesis for 1 μg of extracted total RNA for the RT-qPCR was carried out

using a High Capacity cDNA Reverse Transcription Kit (Applied BioSystems, UK) according to the manufacturer's instructions. The master mix with reverse transcriptase was prepared for all samples (n = 38) adding 2 µL of x10 RT buffer, 0.8 µL dNTP mix (100 mM each), 2 µL 10x RT random primers and 1 µL reverse transcriptase (50 U μL^{-1}) and 4.2 µL nuclease free water. In parallel, two randomly selected samples were prepared using the same master mix but free of reverse transcriptase as an RT- (negative control) to determine genomic contamination. The reverse transcription reaction was then performed by adding samples to a thermocycler (Biometra R) and incubating at 25 °C for 10 min, 37 °C for 2 h and finally 85 °C for 5 min to inactivate the DNA polymerase. The cDNA samples were placed directly on ice for immediate PCR or frozen at -20 °C for later analysis.

Real time qPCR

Primer sequences for the target gene (Na^+/K^+-ATPase) and the reference genes (β-Actin, ELF-1 and Cofilin-2) genes were obtained from Eurofins MWG synthesis GmbH (Ebersberg, Germany) and tested for primer efficiency and quality by generating a standard curve using a pooled cDNA sample prepared from mixing 3 µL of stock cDNA, prior to use in RT-qPCR assay (Table 2) and carrying out melting curve analysis.

The real-time qPCR assay was performed in compliance with MIQE guidelines (Bustin, Benes, Garson, Hellemans, Huggett, Kubista, Mueller, Nolan, Pfaffl, Shipley, Vandesompele, & Wittwer, 2009). The cDNA samples and RT- sample were diluted 1:20 using RNAse free water. For each gene, RT-qPCR assay based on SYBR green chemistry was performed in a Bio-RAD, T100 ™ qPCR machine using white 96-well plates. The RT-qPCR master mix for samples, standard curve (*i.e.* serial dilution of cDNA pool), non-template control (NTC) and internal control (IC) were prepared by mixing 10 µL of Luminaris Color HiGreen qPCR Master

Mix (Fisher Scientific, UK), 1 µL each of Forward Primer and Reverse primer (10 pmol μL^{-1}) and 3 µL of water.

The templates (5 µL) and master mix (15 µL) were loaded into the PCR plate (final volume of 20 µL per sample), before the plate was vortexed (Camlab, UK) and centrifuged by using c1000 Mini Plate Spinner centrifuge. The assay was thermocycled at; UDG pre-treatment at 50 ^{o}C (2 min), an initial denaturation of 95 °C for 10 min, followed by 40 cycles of 95 °C (15 sec), annealing temperature 58 °C (30 sec) and extension 72 °C (30 sec), according to the manufacturer's protocol. The melting curve (dissociation peak) analysis was performed at 70 – 90 °C measuring every 0.5 °C to evaluate primer dimer and genomic contamination.

Gene Expression Analysis

The mean Ct values calculated within the Bio-Rad software were exported to Excel. The gene expression analysis was subsequently carried out using GenEx Enterprise software (version 5.4.3). The expression values (Ct) of the Na^{+}/K^{+}-ATPase were normalised against three reference genes (ELF-1, β-Actin and Cofilin-2, reference gene index). The relative expression value of the test group compared to control (*i.e.* non-AGD challenged) fish was estimated before testing statistical differences between test groups using Minitab® 17 software (Minitab Ltd, Coventry, UK). The normalised mean gene expression values were compared against the control group for any statistical differences using a parametric General Linear Model (GLM) and *post-hoc* test with Bonferroni correction.

Results

Gill histology

Histological examination of samples indicated the presence of AGD-associated focal lesions affecting the secondary lamellae from gills of fish from Groups B-E (n = 5) (Fig. 1).

The histologically observed AGD lesions were graded into 3 different categories, based on their microscopic pathology *i.e.* (A) small focal, (B) medium focal and (C) locally extensive. These were characterised as follows:

1) Small Focal; focal lesions characterised by two different types of pathological findings: 1) Basal hyperplasia; normally involving 2-3 secondary lamellae and variable levels of basal epithelial hyperplasia in the interlamellar space affecting <50 % of the length of the secondary lamellae (Fig. 1A&B). The epithelial cells in the affected areas were marked by hyperplasia and oedema (Fig. 1A&B). 2) Distal lamellar hypertrophy**;** consisting of lamellar swelling and fusion observed at the distal ends of 2-3 secondary lamellae causing the formation of interlamellar lacunae. Such lesions were associated with a varying degree of hyperplasia and intercellular lamellar oedema (Fig. 1A&C).

2) Medium Focal; lesions were defined as segmental lesions affecting between 4-15 secondary lamellae. These lesions were characterised by the presence of marked basal epithelial hyperplasia involving >50 % of the length of the secondary lamellae causing fusion of several lamellae together forming a segment (Fig. 1D). These hyperplastic basal epithelial cells showed hydropic degenerative changes with interstitial and intercellular oedema detected within lesions. Hydropic degeneration of epithelial cells was more marked at the distal end of the secondary lamellae extending proximally to the base, often giving a disruptive look to the epithelial surface of the lesion (Fig. 1D).

3) Locally extensive**;** lesions affecting more than 15 secondary lamellae displayed a complete loss of normal lamellar architecture (Fig. 1E). The affected region included >50 % of the length of the secondary lamellae. The cells were spongiotic and showed both hypertrophic and hyperplastic responses with large areas of degenerated cells and intercellular oedema (Fig. 1E). The marked lamellar hyperplasia resulted in lamellar fusion along the filament which contributed to the 'clubbing' appearance of filaments (not shown). An abundance of mucous cells was detected on the surface of the lesions in close contact with the amoebae (*N. perurans)* (Fig. 1E). Amoebae were often present in surface mucus and were particularly abundant at the site of sloughing surface epithelial cells (Fig. 1E). Figure 1F shows histologically normal gills from a Group A fish.

Semi-quantitative lesion assessment

Based on the semi-quantitative assessment, the number and severity of the focal lesions was seen to be associated with an increase in gross gill score (Fig. 2). As gross gill score increased, there was a shift in the number of observed lesions from small focal to medium focal. Whilst the proportion of lesions was similar in two different groups (Groups B and C), a higher proportion of medium focal lesions was detected in the fish with higher AGD scores (Group D). Within the heavy infection level category (Group E), the overall number of lesions was reduced due to the enlarged surface areas of both medium focal and locally extensive lesions.

Immunohistochemistry

Examination of immunolabeled slides indicated a high specificity of the mouse monoclonal antibody against Na^+/K^+-ATPase for chloride cells in the gills of Atlantic salmon. No cross reactivity was detected from the isotype control or the PBS control.

Based on the observed immunolabeling, chloride cells in non-affected areas of gills were found abundantly distributed at the interlamellar regions and junctions between the filament and lamellae (Fig. 3A). Rarely, chloride cells were found distributed along the lamellae (Fig. 3A). Within the category of lesions classified as 'small focal' (Fig 3B-F), there was a marked reduction in chloride cells in the interlamellar regions, with concurrent mild basal hyperplasia of the epithelium. Multiple oedematous spaces were noted at the sites where chloride cells were previously located (Fig. 3B, C & F). With increasing lesion size, the level of basal hyperplasia was more marked and the hyperplastic region extended across to the interlamellar region of the neighbouring lamellae (Fig. 3E). In these 'small focal' lesions, the number of chloride cells was only markedly reduced at the centre of the lesion (the initial lesion) with intact chloride cells within the neighbouring lamellar region (Fig. 3B, C). These intact chloride cells were lifted distally by the proliferative basal epithelial lining (Fig. 3D). As hyperplasia progressed, sloughing of chloride cells was observed within the lamellar space (Fig. 3E). As the chloride cells moved along the lamellae, signs of hydropic degenerative changes were evident and ultimately replaced by formation of oedematous spaces close to the lesion surface (Fig. 3F).

Depending on the extent of basal proliferation of each interlamellar region, the chloride cells appear only at the border of lesions (Fig. 4A). Throughout the progression of the lesion, minimal regeneration of the chloride cells was observed as no increase in the number of immunolabeled cells was evident. When a distal lamellar hypertrophic lesion was observed, no initial reduction in chloride cells was found in the interlamellar region or filament-lamellar junction (Fig. 4B). When "medium focal" and "locally extensive" lesions were examined, the lesions ranged from minimal immunolabeling at the lesion border to a complete absence of chloride cells within the lesion (Fig. 4C-D).

Transmission Electron Microscopy

Transmission electron microscopy was employed to examine the ultrastructural changes of chloride cells in association with AGD infection by using fish samples from Group A (Infection level category; clear) and Group D (Infection level category; very mild).

Normally appearing chloride cells from the uninfected gill tissues were characterised by their columnar shape, high numbers of electron dense mitochondria and a well-developed vesicular tubular network in close association with the endoplasmic reticulum in the cytoplasm (Fig. 5A, B). At the apical portion of the cell, vesicles and short tubules replace the more extensive intricate vesicular tubular network of the basolateral portion (Fig. 5C). Mitochondria were characterised by a well demarcated double enveloped membrane with well-defined infoldings of cristae closely linked to the inner membrane of the mitochondria (Fig. 5D).

The surface of the gill lamellae in fish from Group D appeared oedematous with multiple areas of epithelial hyperplasia. In some areas, there was separation of epithelial lining from the basement membrane due to intercellular oedema (Fig. 6A). Hydropic degeneration was evident in multiple chloride cells on the lamellar surface, recognised by cell swelling, electron lucent cytoplasm due to the formation of multiple vacuoles and marked loss of endoplasmic tubular details (Fig. 6B). On the apical membrane, there was the fusion and loss of microridges (Fig. 6C). The swollen mitochondria were characterised by an ill-defined envelope, an electron lucent matrix and distorted cristae. (Fig. 6D).

Real-time-qPCR of *P. perurans* quantification and Na^+/K^+-ATPase gene expression

The real-time qPCR results for *P. perurans* quantification and Na^+/K^+-ATPase relative expression assays are shown in Figs. 7 and 8 respectively. An increase in *P. perurans* load is seen to correlate with an increase in gross gill scores (Fig. 7). However the Group A (clear) fish, who displayed no macroscopic gross gill scores to suggest AGD infection,

exhibited a low level of genomic *N. perurans* DNA equivalents (Fig. 7A). The likely reason for this is the non-experimentally challenged fish, from which Group A were selected, had come into previous contact with *N. perurans* through the inlet water supply pumped directly from the sea at the research facility. Fish had been treated with freshwater two weeks prior to this experiment.

The relative expression level of Na^+/K^+-ATPase transcript (Fig. 8) was notably down-regulated in AGD-challenged fish compared to fish from the non-experimentally challenged group (Group A), with the exception of Group B (Very Light; AGD score: 0-0.5; $n = 5$) (L; tissues from lesion site) (Fig. 7B).

Interestingly both the amoebic load (Fig. 7) and the level of Na^+/K^+-ATPase (Fig. 8) gene expression in tissues from lesion site (L) and apparently normal tissues from adjacent to lesion site (N) were not found to be statistically different.

Discussion

There have been limited studies to date focusing on the implications of early stage AGD in Atlantic salmon. Considering the variable efficacy of hydrogen peroxide treatment (Adams, Crosbie, & Nowak, 2012; Powell & Clark, 2003) the logistic and economic problems associated with freshwater treatment (Nowak, 2012) and the difficulty of controlling the disease at higher temperatures, early detection and prevention are critical for AGD management in commercial Atlantic salmon aquaculture. Therefore, a better understanding of early stage AGD-associated gill lesions is crucial to the timely management of the disease.

457 The histopathological findings from the present work resembled common findings in
458 previously published AGD studies *i.e.* variable levels of basal epithelial hyperplasia and
459 subsequent lamellar fusion, which became increasingly extensive as the lesion advances
460 (Munday, Foster, Roubal & Lester 1990; Nowak & Munday 1994; Adams & Nowak 2001;
461 Adams, Ellard & Nowak 2004). Ultrastructural examination of gill epithelium and chloride
462 cells in AGD infected gills using TEM revealed signs of oedema and epithelial
463 hyperplasia, even in fish scored as having very mild AGD lesions (Group D). The observed
464 hydropic degeneration and loss of apical microridges in CCs strongly suggest the
465 likelihood of severe functional impairment, even where CCs are still visible by light
466 microscopy, and could have implications for ion and pH regulation in these fish and thus
467 for wider health and welfare indicators (Van Der Heijden et al., 1999).
468
469 In the present study, histological assessment of AGD-related lesions corresponded well to
470 the qPCR *P. perurans* quantification; for example, the increased levels of *P. perurans* in
471 Group D (very mild; gross gill score: 1.0-1.5) and Group E (heavy; gross gill score 3.5-
472 4.5) compared to Group A (clear; gross gill score 0) was supported by the increased
473 number of medium focal and locally extensive lesions within these groups when compared
474 to Group A. However, a disparity has previously been reported between diagnostic
475 methods used for AGD; Atlantic salmon gills displaying grossly visible lesions did not
476 show the presence of *P. perurans* at a histological level, with this discrepancy deemed
477 likely to be due to the sampling technique during gill excision *i.e.* only one section from
478 one gill arch was examined for subsequent histological analysis (Clark & Nowak, 1999)
479 and also loss of mucus and associated amoebae during fixation. It is indeed well
480 established that conventional fixatives often wash away the overlaying mucus layers (Lee
481 Schurch, Roth, Jiang, Cheng, Bjarnason & Green, 1995; Mays, Feldhoff, & Nettleton, 1984)

and associated amoebae, hence the need for alternative methods to optimise fixation to enable mucus stabilisation and allow a better understanding of parasite interactions with gill mucus during AGD infection (Fernandez, Mascolo, Monaghan, Baily, Chalmers, Paladini, Adams, Bron, & Fridman, 2019). In the current study, gills for subsequent downstream molecular analysis of *P. perurans* load was taken from a section of gill displaying grossly visible AGD lesions which would most likely account for the correlation seen.

The identification of *P. perurans* by molecular analysis in fish from Group A (no macroscopic signs of infection) is in agreement with previous studies where grossly visible white patches, used for presumptive diagnosis were not found in AGD infected rainbow trout (*Onchorhynchus mykiss*) (Munday, Foster, Roubal, & Lester, 1990) and Atlantic salmon (Clark & Nowak, 1999) suggesting this method is only reliable in cases of heavy AGD infection. When appraising the findings of this study, it is vital to evaluate the experimental limitations. As the results indicated, the control fish (Group A) were not free from AGD as both *P. perurans* loads and histological AGD lesions were detected from the samples. This was due to the presence of *P. perurans* in the inlet water resulting in a naturally occurring infection. At present, there is a shortage of commercial AGD- specific pathogen free fish. Many current studies are being carried out to explore the possibility of selective breeding for AGD resistance as there is evidence of heritable genetic variation in AGD susceptibility in both survival and gross gill pathology (Taylor, Kube, Muller, & Elliott, 2009). In addition, in the current study, non-specific chronic gill changes were present on occasion amongst fish within different AGD score groups which were characterised by the presence of remodeling and healing fractures of gill cartilage surrounded by fibrotic capsules of collagen and hyperplastic epithelial tissues indicating the chronic nature of these

pathologies. It was difficult to ascertain the causative agent for these types of lesions however fish from the present study had previously been infected with AGD and underwent freshwater treatment prior to the commencement of this cohabitation trial. It is most likely that this cartilage remodelling represents chronic changes associated with previously severe AGD infection.

Immunohistochemistry was used to examine distributional changes of chloride cells in relation to AGD lesion development in the current study. The decrease in chloride cell numbers was closely associated with the degree of basal epithelial hyperplasia. There was an initial focal loss of chloride cells (from 1-2 inter-lamellar spaces) where minimal basal epithelial hyperplastic changes were observed, suggesting the possible presence of localised irritants such as the attachment of *P. perurans*. Previous studies have noted that the subsequent development and progression of the lesion relies on the host's proliferative response and migration of amoebae along the filament (Taylor, Muller, Cook, Kube, & Elliott, 2009). As the level of basal epithelial hyperplasia increased at the centre of the lesions, hydropic degeneration of the chloride cells was observed, which ultimately led to formation of regional oedema and sloughing of degenerated chloride cells on the surface of the lesions. The subsequent presence of chloride cells towards the distal end of the lamellae was in accordance with previous reports in Atlantic salmon (Chalmers et al., 2017).

It has been previously reported that no overall reduction in chloride cells was evident from 'mild' and 'moderate' infected fish by quantitative digital image analysis from a re-infection AGD field trial (Adams & Nowak, 2003). This was most likely due to the localised nature of the lesions which appeared in small numbers on the gill and thus had

very limited effect on the overall chloride cell numbers of the gills. In the current study, by the time AGD lesions advanced to 'medium focal' or 'locally extensive' lesions, the chloride cells were almost completely absent from these hyperplastic areas. The reduction in chloride cells in the hyperplastic AGD lesions observed in the current study is supported by previous studies (Adams & Nowak, 2003; Munday et al., 1990; Nowak & Munday, 1994; Roubal, Lester, & Foster, 1989).

Chloride cells are characterised by a columnar/ovoid appearance, sharing the same ultrastructural features as other ion transport cells *e.g.* high mitochondrial density and a well-developed vesicular-tubular network, which is continuous with the extensively invaginated basolateral membrane (Van Der Heijden,Van Der Meij, Flik, & Wendelaar Bonga, 1999). The extensive vesicular-tubular network within the cytoplasm provides a large surface area for the ion-transport protein, Na^+/K^+-ATPase (Perry, 1997). Chloride cells are believed to be the primary extra-renal site for regulation of osmotically active ion concentrations, ultimately helping to regulate blood pH by manipulating the rates of Cl^- and Na^+ ionic uptake, the activity of which mediates transfer of H^+ and HCO_3^- (Evans, Piermarini, & Choe, 2005; Laurent & Dunel, 1980). Apoptosis of CCs in teleosts has been previously described under both pathogenic conditions *i.e.* toxicants in the rainbow trout (*O. mykiss*) (Daoust, Wobeser, & Newstead, 1984; Mallat, 1985) and under physiological conditions in newly hatched rainbow trout (Rojo, & Gonzalez, 1999), newly hatched brown trout (*S. trutta*) (Rojo, Blanquez, & Gonzalez, 1997), the adult Mozambique tilapia (*O. mossambicus*) (Wendelaar Bonga & van der Meij, 1989; Wendelaar Bonga, Flik, Balm, & van der Meij, 1990) and the hybrid *O. mossambicus* x *Oreochromis urolepis hornorum* (Sardella, Maey, Cooper, Gonzalez, & Brauner, 2004). These authors all report the ultrastructural changes of MRCs as showing nuclear and cytoplasmic condensation and enlargement of the

557 mitochondria surrounded by a distended tubular system and oedematous areas, as reported in
558 the current study. In addition intracellular oedema caused a lifting of the epithelial lining and
559 loss of microridges was apparent.
560 To conclude, this study has added to pre-existing knowledge of host-pathogen interactions
561 underlying the early stages of AGD infection in Atlantic salmon and identified
562 distributional and morphological changes of chloride cells associated with them. A marked
563 reduction in chloride cells (*i.e.* Na^+/K^+-ATPase immunolabeling) was detected at the
564 interlamellar region of the gills and found to be closely linked to increasing levels of basal
565 epithelial hyperplasia from focal AGD lesions. Acute degenerative changes in chloride
566 cells at the lesion site were recognised by the use of TEM indicating cytoplasmic
567 condensation, and oedematous areas and microridge changes. Both distributional and
568 morphological changes were supported by the early onset down-regulation of Na^+/K^+-
569 ATPase gene expression. This work provides useful information about the effects of host-
570 pathogen interaction during AGD infection at a cellular level and their pathophysiological
571 implications.
572
573 **References**
574 Adams, M. B., Crosbie, P. B. B., & Nowak, B. F. (2012). Preliminary success using
575 hydrogen peroxide to treat Atlantic salmon, *Salmo salar* L., affected with
576 experimentally induced amoebic gill disease (AGD). *Journal of Fish Diseases*, *35*(11),
577 839–848. http://doi.org/10.1111/j.1365-2761.2012.01422.x
578 Adams, M. B., Ellard, K., & Nowak, B. F. (2004). Gross pathology and its relationship with
579 histopathology of amoebic gill disease (AGD) in farmed Atlantic salmon, *Salmo salar*
580 L. *Journal of Fish Diseases*, *27*, 151–161.
581 Adams, M. B., & Nowak, B. F. (2001). Distribution and structure of lesions in the gills of

582 Atlantic salmon, *Salmo salar* L., affected with amoebic gill disease. *Journal of Fish*
583 *Diseases*, *24*(9), 535–542. http://doi.org/10.1046/j.1365-2761.2001.00330.x
584 Adams, M. B., & Nowak, B. F. (2003). Amoebic gill disease: sequential pathology in
585 cultured Atlantic salmon, *Salmo salar* L. *Journal of Fish Diseases*, *26*, 601–614.
586 Retrieved from http://doi.wiley.com/10.1111/j.1365-2761.2004.00531.x
587 Bustin, S. A., Benes, V., Garson, J. A., Hellemans, J., Huggett, J., Kubista, M., … Wittwer,
588 C. T. (2009). The MIQE guidelines: Minimum information for publication of
589 quantitative real-time PCR experiments. *Clinical Chemistry*, *55*(4), 611–622.
590 http://doi.org/10.1373/clinchem.2008.112797
591 Bustos, P. A., Young, N. D., Rozas, M. A., Bohle, H. M., Ildefonso, R. S., Morrison, R. N.,
592 & Nowak, B. F. (2011). Amoebic gill disease (AGD) in Atlantic salmon (*Salmo salar*)
593 farmed in Chile. *Aquaculture*, *310*, 281–288.
594 http://doi.org/10.1016/j.aquaculture.2010.11.001
595 Chalmers, L., Taylor, J. F., Roy, W., Preston, A. C., Migaud, H., & Adams, A. (2017). A
596 comparison of disease susceptibility and innate immune response between diploid and
597 triploid Atlantic salmon (*Salmo salar*) siblings following experimental infection with
598 Neoparamoeba perurans, causative agent of amoebic gill disease. *Parasitology*, *144*(09),
599 1229–1242. http://doi.org/10.1017/S0031182017000622
600 Clark, A., & Nowak, B. F. (1999). Field investigations of amoebic gill disease in Atlantic
601 salmon, *Salmo salar* L., in Tasmania. *Journal of Fish Diseases*, *22*(6), 433–443.
602 http://doi.org/10.1046/j.1365-2761.1999.00175.x
603 Daoust, P. Y., Wobeser, G., & Newstead, J. D. (1984). Acute pathological effects of
604 inorganic mercury and copper in gills of rainbow trout. *Veterinary Pathol*ogy, *21*, 93–
605 101.
606 Downes, J., Henshilwood, K., Collins, E., Ryan, A., O'Connor, I., Rodger, H., … Ruane, N.

(2015). A longitudinal study of amoebic gill disease on a marine Atlantic salmon farm utilising a real-time PCR assay for the detection of *Neoparamoeba perurans*. *Aquaculture Environment Interactions*, *7*(3), 239–251. http://doi.org/10.3354/aei00150

Evans, D. H., Piermarini, P. M., & Choe, K. P. (2005). The multifunctional fish gill: dominant site of gas exchange, osmoregulation, acid-base regulation, and excretion of nitrogenous waste. *Physiological Reviews*, *85*, 97–177. http://doi.org/10.1152/physrev.00050.2003.

Fernandez, C., Mascolo, D., Monaghan, S. J., Baily, J. L., Chalmers, L., Paladini, G., … Fridman, S. (2019). Methacarn preserves mucus integrity and improves visualization of amoebae in gills of Atlantic salmon (*Salmo salar* L.). *Journal of Fish Diseases*, (April), jfd.12988. http://doi.org/10.1111/jfd.12988

Findlay, V. L., & Munday, B. L. (1998). Further studies on acquired resistance to amoebic gill disease (AGD) in Atlantic salmon, *Salmo salar* L. *Journal of Fish Diseases*, *21*(2), 121–125. http://doi.org/10.1046/j.1365-2761.1998.00086.x

Haugland, G. T., Olsen, A. B., Rønneseth, A., & Andersen, L. (2017). Lumpfish (*Cyclopterus lumpus* L.) develop amoebic gill disease (AGD) after experimental challenge with *Paramoeba perurans* and can transfer amoebae to Atlantic salmon (*Salmo salar* L.). *Aquaculture*, *478*, 48–55. http://doi.org/10.1016/j.aquaculture.2016.04.001

Herath, T. K., Bron, J. E., Thompson, K. D., Taggart, J. B., Adams, A., Ireland, J. H., & Richards, R. H. (2012). Transcriptomic analysis of the host response to early stage salmonid alphavirus (SAV-1) infection in Atlantic salmon *Salmo salar* L. *Fish and Shellfish Immunology*, *32*(5), 796–807. http://doi.org/10.1016/j.fsi.2012.02.001

Karlsbakk, E., Olsen, A. B., Einen, A.-C. B., Mo, T. A., Fiksdal, I. U., Aase, H., … Hansen, H. (2013). Amoebic gill disease due to *Paramoeba perurans* in ballan wrasse (*Labrus bergylta*). *Aquaculture*, *412–413*, 41–44.

http://doi.org/10.1016/j.aquaculture.2013.07.007

Laurent, P., & Dunel, S. (1980). Morphology of gill epithelia in fish. *American Journal of Physiology-Regulatory, Integrative and Comparative Physiology*, *238*(3), R147–R159. http://doi.org/10.1152/ajpregu.1980.238.3.R147

Lee, M. M., Schurch, S., Roth, S. H., Jiang, X., Cheng, S., Bjarnason, S., & Green, F. H. Y. (1995). Effects of acid aerosol exposure on the surface properties of airway mucus. *Experimental Lung Research*, *21*(6), 835–851. http://doi.org/10.3109/01902149509031766

Madsen, S. S., Kiilerich, P., & Tipsmark, C. K. (2009). Multiplicity of expression of Na+,K+-ATPase alpha-subunit isoforms in the gill of Atlantic salmon (*Salmo salar*): cellular localisation and absolute quantification in response to salinity change. *Journal of Experimental Biology*, *212*, 78–88. http://doi.org/10.1242/jeb.024612

Mallat, J. (1985). Fish gill structural changes induced by toxicants and other irritants: a statistical review. *Canadian Journal of Fish and Aquatic Sciences,* 42**,** 630–648.

Mays, E. T., Feldhoff, R. C., & Nettleton, G. S. (1984). Determination of protein loss during aqueous and phase partition fixation using formalin and glutaraldehyde. *Journal of Histochemistry and Cytochemistry*, *32*(10), 1107–1112. http://doi.org/10.1177/32.10.6434629

Morais, S., Monroig, O., Zheng, X., Leaver, M. J., & Tocher, D. R. (2009). Highly unsaturated fatty acid synthesis in Atlantic salmon: Characterization of ELOVL5- and ELOVL2-like elongases. *Marine Biotechnology*, *11*(5), 627–639. http://doi.org/10.1007/s10126-009-9179-0

Mouton, A., Crosbie, P., Cadoret, K., & Nowak, B. (2014). First record of amoebic gill disease caused by *Neoparamoeba perurans* in South Africa. *Journal of Fish Diseases*, *37*(4), 407–409. http://doi.org/10.1111/jfd.12133

Munday, B. L. (1986). Diseases in salmonids. In J. D. Humphrey & J. S. Landon (Eds.), *Diseases of Australian Fish and Shellfish* (pp. 127–141). Victoria: Department of Agriculture and Rural Affairs.

Munday, B. L., Foster, C. K., Roubal, F. R., & Lester, R. J. G. (1990). Paramoebic gill infection and associated pathology of Atlantic salmon, *Salmo salar* and rainbow trout, *Salmo gairdneri* in Tasmania. In F. O. Perkins & T. C. Cheng (Eds.), *Pathology in Marine Science* (pp. 215–222). San Diego: Academic Press. http://doi.org/10.1016/B978-0-12-550755-4.50026-4

Munday, B. L., Zilberg, D., & Findlay, V. (2001). Gill disease of marine fish caused by infection with *Neoparamoeba pemaquidensis*. *Journal of Fish Diseases*, *24*(9), 497–507. http://doi.org/10.1046/j.1365-2761.2001.00329.x

Nowak, B. F. (2012). *Neoparamoeba perurans*. In P. T. K. Woo & K. Buchmann (Eds.), *Fish parasites: pathobiology and protection* (1st ed.). London: CABI International.

Nowak, B. F., & Munday, B. L. (1994). Histology of gills of Atlantic salmon during the first few month following transfer to sea water. *Bulletin of the European Association of Fish Pathologists*, *14*(3), 77–81.

Oldham, T., Rodger, H., & Nowak, B. F. (2016). Incidence and distribution of amoebic gill disease (AGD) - An epidemiological review. *Aquaculture*, *457*, 35–42. http://doi.org/10.1016/j.aquaculture.2016.02.013

Perry, S. F. (1997). The chloride cell: Structure and function in the gills of freshwater fishes. *Annual Review of Physiology*, *59*(9), 325–347. http://doi.org/10.1146/annurev.physiol.59.1.325

Powell, M. D., & Clark, G. A. (2003). In vitro survival and the effect of water chemistry and oxidative chemical treatments on isolated gill amoebae from AGD-affected Atlantic salmon. *Aquaculture*, *220*(1–4), 135–144. http://doi.org/10.1016/S00448486(02)006294

682 Rodger, H. D. (2014). Amoebic gill disease (AGD) in farmed salmon (*Salmo salar*) in
683 Europe. *Fish Veterinary Journal*, *14*, 16–27.
684 Rodger, H. D., & McArdle, J. F. (1996). An outbreak of amoebic gill disease in Ireland.
685 *Veterinary Record*, *139*(14), 348–349. http://doi.org/10.1136/vr.139.14.348
686 Rojo, C., & González, E. (1999). Ontogeny and apoptosis of chloride cells in the gill
687 epithelium of newly hatched rainbow trout. *Acta Zoologica*, *80*, 11–23.

688 Rojo, M.C., Blanquez, M.J., & Gonzalez, M.E. (1997). Ultrastructural evidence for apoptosis
689 of pavement cells, chloride cells and hatching gland cells in the developing branchial
690 area of the trout *Salmo trutta*. *Journal of Zooogy, 243*, 637-651.

691 Roubal, F. R., Lester, R. J. G., & Foster, C. K. (1989). Studies on cultured and gill-attached
692 *Paramoeba* sp. (Gymnamoebae: Paramoebidae) and the cytopathology of paramoebic
693 gill disease in Atlantic salmon, *Salmo salar* L., from Tasmania. *Journal of Fish*
694 *Diseases*, *12*(5), 481–492. http://doi.org/10.1111/j.1365-2761.1989.tb00559.x
695 Sardella, B., Matey, V., Cooper, J., Gonzalez, R. and Brauner, C. (2004). Physiological,
696 biochemical and morphological indicators of osmoregulatory stress in 'California'
697 Mozambique tilapia (*Oreochromis mossambicus* × *O. urolepis hornorum*) exposed to
698 hyper saline water. *Journal of Experimental Biology*, *207*, 1399–1413.
699 Shinn, A. P., Pratoomyot, J., Bron, J. E., Paladini, G., Brooker, E. E., & Brooker, A. J.
700 (2015). Economic costs of protistan and metazoan parasites to global mariculture.
701 *Parasitology*, *142*, 196–270. http://doi.org/10.1017/S0031182014001437
702 Speare, D. J., Arsenault, G., MacNair, N., & Powell, M. D. (1997). Branchial lesions
703 associated with intermittent formalin bath treatment of Atlantic salmon, *Salmo salar* L.,
704 and rainbow trout, *Oncorhynchus mykiss* (Walbaum). *Journal of Fish Diseases*, *20*(1),
705 27–33. http://doi.org/10.1046/j.1365-2761.1997.d01-103.x

706 Steinum, T., Kvellestad, A., Rønneberg, L. B., Nilsen, H., Asheim, A., Fjell, K., … Dale, O.
707 B. (2008). First cases of amoebic gill disease (AGD) in Norwegian seawater farmed
708 Atlantic salmon, *Salmo salar* L., and phylogeny of the causative amoeba using 18S
709 cDNA sequences. *Journal of Fish Diseases*, *31*(3), 205–214.
710 http://doi.org/10.1111/j.1365-2761.2007.00893.x
711 Taylor, R. S., Kube, P. D., Muller, W. J., & Elliott, N. G. (2009). Genetic variation of gross
712 gill pathology and survival of Atlantic salmon (*Salmo salar* L.) during natural amoebic
713 gill disease challenge. *Aquaculture*, *294*(3–4), 172–179.
714 http://doi.org/10.1016/j.aquaculture.2009.06.007
715 Taylor, R. S., Muller, W. J., Cook, M. T., Kube, P. D., & Elliott, N. G. (2009). Gill
716 observations in Atlantic salmon (*Salmo salar,* L.) during repeated amoebic gill disease
717 (AGD) field exposure and survival challenge. *Aquaculture*, *290* (1–2), 1–8.
718 http://doi.org/10.1016/j.aquaculture.2009.01.030
719 Van Der Heijden, A. J. H., Van Der Meij, J. C. A., Flik, G., & Wendelaar Bonga, S. E.
720 (1999). Ultrastructure and distribution dynamics of chloride cells in tilapia larvae in
721 fresh water and sea water. *Cell and Tissue Research*, *297*(1), 119–130.
722 http://doi.org/10.1007/s004410051339
723 Wendelaar Bonga, S.E. and van der Meij, J.C.A. (1989). Degeneration and death by
724 apoptosis and necrosis of the pavement and chloride cells in the gills of the teleost.
725 *Cell Tissue Research*, *255*, 235–243.
726 Wendelaar Bonga, S.E., Flik, G., Balm, P.H.M. and van der Meij, J.C.A. (1990). The
727 ultrastructure of chloride cells in the gills of the teleost *Oreochromis mossambicus*
728 during exposure to acidified water. *Cell Tissue Res*. *259* (575–585).
729
730 Wilson, J. M., & Laurent, P. (2002). Fish gill morphology: Inside out. *Journal of*

Experimental Zoology, *293*(3), 192–213. http://doi.org/10.1002/jez.10124

Young, N. D., Crosbie, P. B. B., Adams, M. B., Nowak, B. F., & Morrison, R. N. (2007). *Neoparamoeba perurans* n. sp., an agent of amoebic gill disease of Atlantic salmon (*Salmo salar*). *International Journal for Parasitology*, *37*(13), 1469–1481. http://doi.org/10.1016/j.ijpara.2007.04.018

Figure legends

Figure 1. Histology of AGD infected Atlantic salmon gills following cohabitation challenge. A) Section of gills from infected Atlantic salmon from Group D (gross gill score: 1.0-1.5). An example of focal basal hyperplasia occupying <50% of the length of the secondary lamellae (upper box) and distal lamellar fusion occupying < 50% lamellae of the length of the secondary lamellae (lower box) (bar = 50μm); B) Higher magnification of A) (upper box). *Note* the formation of intercellular oedema (OE) (asterisks) (bar = 10μm); C) Higher magnification of A) (lower box). *Note* formation of lacunae (L) (bar = 10μm); D) Section of gills from infected Atlantic salmon from Group C (gross gill score: 0.5-1.0). An example of a medium focal lesion involving more than three lamellae and extending > 50% of lamellae length (bar = 50μm). Insert; higher magnification of boxed area. The lesion involves multiple epithelial cells undergoing hydropic degeneration and extensive areas of intercellular oedema (asterisks) contributing to the disruption of the lesion surface (bar = 20μm); (E) Section of gill from infected Atlantic salmon from Group E (gross gill score: 3.5-4.5). An example of a locally extensive lesion illustrating the total loss of normal gill architecture. The presence of *Neoparamoebae* sp. associated with the sloughing epithelium (arrows) (bar = 500μm); F) Section of histologically normal gill from Atlantic salmon from Group A (bar = 500μm).

Figure 2. Quantification and qualification of lesions in AGD infected gills tissue of Atlantic salmon. Group A: clear; Group B: very light; gross gill score 0-0.5, Group C: light; gross gill score 0.5-1, Group D: very mild; gross gill score1-1.5; Group E: heavy; gross gill score 3.5 – 4.5 (n = 3 per group). There is a positive link between gross gill scores and the number and severity of the lesions in the low-grade AGD groups. In the heavy infection level category

(Group E), lesions were much reduced in number due to the larger surface area exhibited by the more severe lesions.

Figure 3. Immunohistochemistry of AGD-affected Atlantic salmon gills following cohabitation challenge showing immunolabeled chloride cells within 'small focal' lesions. Micrographs B-F are from gills of AGD infected fish from Group D exhibiting gross gill scores of 1-1.5. A) Localised Na^+/K^+-ATPase immunolabeling of normal chloride cells from a Group A fish. The positive immunolabeled cells are predominately distributed on interlamellar regions. A few chloride cells were also noted along the lamellae (arrow) (bar = 50 μm); B) Absence of Na^+/K^+-ATPase immunolabeling at interlamellar regions of lesion site where minimal basal lamellar hyperplasia was detected (arrowheads). Visible intra-epithelial oedema at the areas where the chloride cells were previously located (OE) (arrows) (bar = 50μm); C) Hyperplastic areas demonstrating the formation of intra-epithelial oedema where the chloride cells were previously located (arrows) (bar= 50μm); D) The hyperplastic region can be seen to extend to the neighbouring inter-lamellar space (arrows) due to a more pronounced basal lamellar hyperplasia. Note the complete loss of immunolabeled chloride cells occurring at the centre of lesions (asterisk) (bar = 50μm); E) With more pronounced hyperplasia, the reduction in number of immunolabeled chloride cells extends to the neighbouring hyperplastic interlamellar space. Note the sloughing chloride cell (arrow) (bar = 50μm); F) Inter and intracellular oedema (OE) (arrows) and sloughing chloride cell (arrowhead) at the surface of the hyperplastic region (bar = 50μm).

Figure 4. Immunohistochemistry of AGD-affected Atlantic salmon gill following cohabitation challenge showing immunolabeled chloride cell within 'small focal', 'medium focal' and 'locally extensive' lesions. Micrographs A-C are from gills of AGD infected fish

from Group D exhibiting gross gill scores of 1-1.5 and micrograph D is from gills of AGD infected fish from Group E exhibiting gross gill scores of 3.5-4.5. A) An example of a 'medium focal' lesion. Basal hyperplasia has resulted in almost complete fusion of the lamellae with resulting lack of immunolabeled chloride cells at the lesion site. Note the distal location of chloride cells on periphery of hyperplastic regions (asterisk) (bar = 50um); B) An example of a mixed 'small focal' lesion involving both basal lamellar hyperplasia and distal lamellar hypertrophy. Note the formation of the lacunae (L) (bar = 50μm); C) Extensive lack of immunoreactivity throughout the 'medium focal' lesion. Note sparse distribution of immunolabeled chloride cells at the edge of the lesion (arrows) (bar = 50μm); D) An example of a 'locally extensive' lesion showing a few isolated, immunolabeled, hypertrophic chloride cells (arrows) within the filament which is markedly expanded by epithelial hyperplasia (bar = 50μm).

Figure 5.Transmission Electron Micrographs of Atlantic salmon gill filaments of Group A fish (clear). A) A multi-cellular complex consisting of central chloride cell (CC) with adjacent accessory cells (AC). Normal chloride cell structure is characterised by a columnar appearance with microridges (MR) present on the apical surface, a high mitochondrial density (M) and an extensive vesicular tubular network (T) (bar = 2μm); B) An interlamellar space showing microridges (MR), an epithelial pavement cell (PVC), a mucous cell (MC) and chloride cells (CC) (bar = 2μm); C) Higher magnification of the apical portion of a chloride cell, where vesicles (V) and shorter tubules (TS) replace the more extensive intricate vesicular tubular network of the basolateral portion (bar = 390nm); D) Higher magnification of the basolateral portion of a chloride cell. Mitochondria (M), characterised by a double-membraned envelope and an electron dense matrix which containing infoldings of cristae (C),

are surrounded by well-developed vesicular tubular network in close association with the endoplasmic reticulum (ER) (bar = 290nm).

Figure 6. Transmission electron micrographs of Atlantic salmon gill filaments from Group D fish (gross gill score 1-1.5). A) Degenerative changes of a secondary lamella; areas of mild hyperplasia (arrowheads) include chloride cells (CC) and epithelial pavement cells (PVC) displaying vacuole formation within the cells and oedema (OE) at the space between lamellar epithelial cells and the basement membrane, resulting in separation of the epithelial cells from the basement membrane (arrow). Note pillar cells (PC) and intraluminal red blood cells (RBC) (bar = 5μm); B) An example of chloride cell degeneration; a swollen and vacuolated cell undergoing hydropic degeneration. The cytoplasm is pale due to swelling of intracellular organelle structures *i.e.* vesicular tubular system and electron dense mitochondria. The nucleus (N) is also pale. The microridges are intact but there is evidence of areas of fusion (FMR) (bar = 2μm); C) Micrograph showing the complete loss (arrow) and fusion (arrowheads) of microridges. A large vacuole (V) has formed in the cytoplasm due to hydropic degenerative changes (bar = 2μm); D) A higher magnification of cytoplasm of a degenerating CC showing oedema (OE) and swelling of the mitochondria (M); both the loss of electron density of the matrix and the loss of cristae is observed. Swelling and disorganization of the vesicular tubular network is evident (bar = 290nm).

Figure 7. Graph showing increasing *N. perurans* loads with increasing AGD gross gill scores in Atlantic salmon gills, expressed as *N. perurans* genomic equivalents $50ng^{-1}$ total DNA. Group A (clear; gross gill score: 0); Group B (very light, gross gill score: 0-0.5); Group C

(light; gross gill score: 0.5-1.0); Group D (very mild; gross gill score: 1.0-1.5); Group E (heavy; from archival sample; gross gill score: 3.5-4.5). Sample type L = taken from area of visible lesion; N = taken from area with no visible lesion. Groups B-D; L samples (n = 5 per group except Group D which was n = 4) and N samples (n = 5 per group except Group D which was n = 4). Group A samples consisted of pooled biopsies taken from 2 different sites on the gill (n = 5). Group E was a single sample taken from a visible lesion (n = 5). Values are expressed as mean ± SE. Letters on graph indicate values that were significantly different (Mann Whitney-U, $p < 0.05$).

Figure 8. Graph showing relative real-time qPCR quantification of Na^+/K^+-ATPase gene expression. Na^+/K^+-ATPase gene expression was calibrated relative to fish from Group A (clear). Values are expressed as mean ± SE. Letters on graph indicate values that were significantly different (parametric general linear model, $p = <0.0001$).

Table 1

Categorised groups corresponding to infection level category of amoebic gill disease and the corresponding gill score (Taylor, Muller, Cook, Kube, & Elliott, 2009) of fish from the current study.

Group	Infection level category	Gross AGD gill score
A	Clear	0
B	Very light	0 – 0.5
C	Light	0.5 - 1
D	Very mild	1 – 1.5
E†	Heavy	3.5 – 4.5

† refers to archival samples.

Table 2 qPCR primers sequence for Na^+/K^+-ATPase gene expression analysis

Transcript	Primer Name	Primer sequence	Efficiency	Source
Target Genes				
Na^+/K^+-ATPase	As_NaK_β1_F	CCAATGAAAGCATCCCTAG	0.99	Madsen, Kiilerich, & Tipsmark (2009)
	As_Nak_ β1_R	GGCGTCCTCCTCTCTCTTGT		
Reference Genes				
ELF-1	As_ELF1_F	CTGCCCCTCCAGGACGTTTACAA	0.99	Morais, Monroig, Zheng, Leaver, & Tocher (2009)
	As_ELF1_R	CACCGGGCATAGCCGATTCC		
Cofilin-2	As_Cofilin2_F	AGCCTATGACCAACCCACTG	0.97	Herath, Bron, Thompson, Taggart, Adams, Ireland, & Richards, (2012)
	As_Cofilin2_R	TGTTCACAGCTCGTTTACCG		
β actin	As_actin_F	ACTGGGACGACATGGAG	0.96	Morais Monroig, Zheng, Leaver, & Tocher (2009)
	As_actin_R	GGGGTGTTGAAGGTCTC		

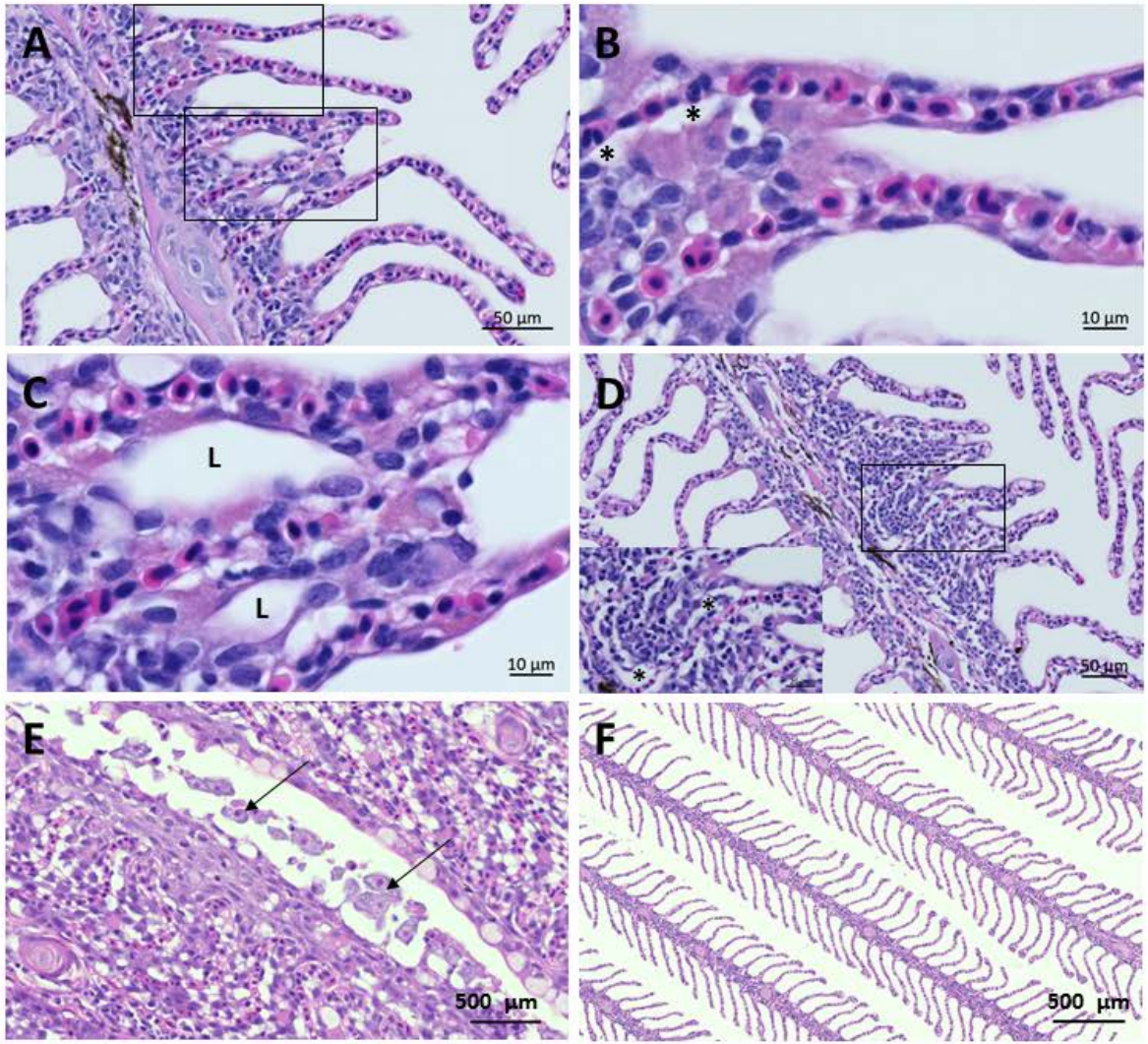
A
50 µm
B
*
*
10 µm
C
L
L
10 µm
D
*
*
50 µm
E
500 µm
F
500 µm

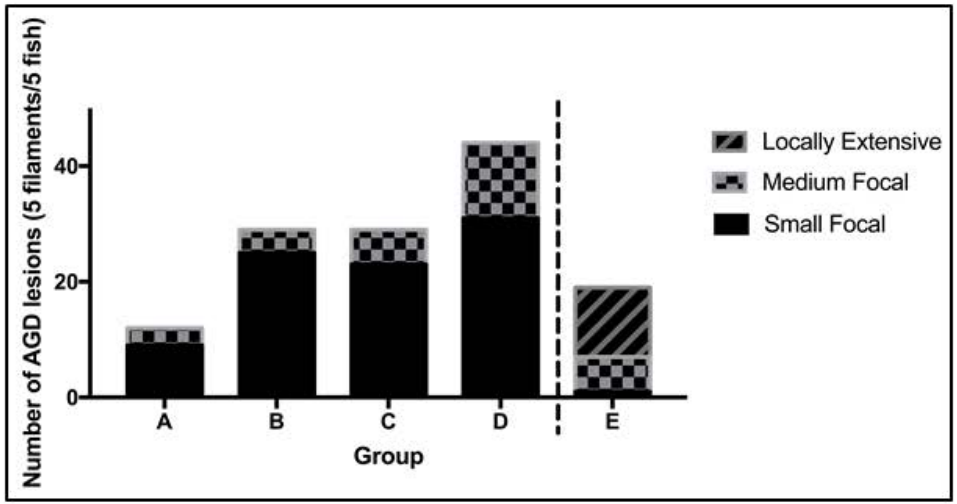
Number of AGD lesions (5 filaments/5 fish)
40
20
0
A
B
C
D
E
Group
Locally Extensive
Medium Focal
Small Focal

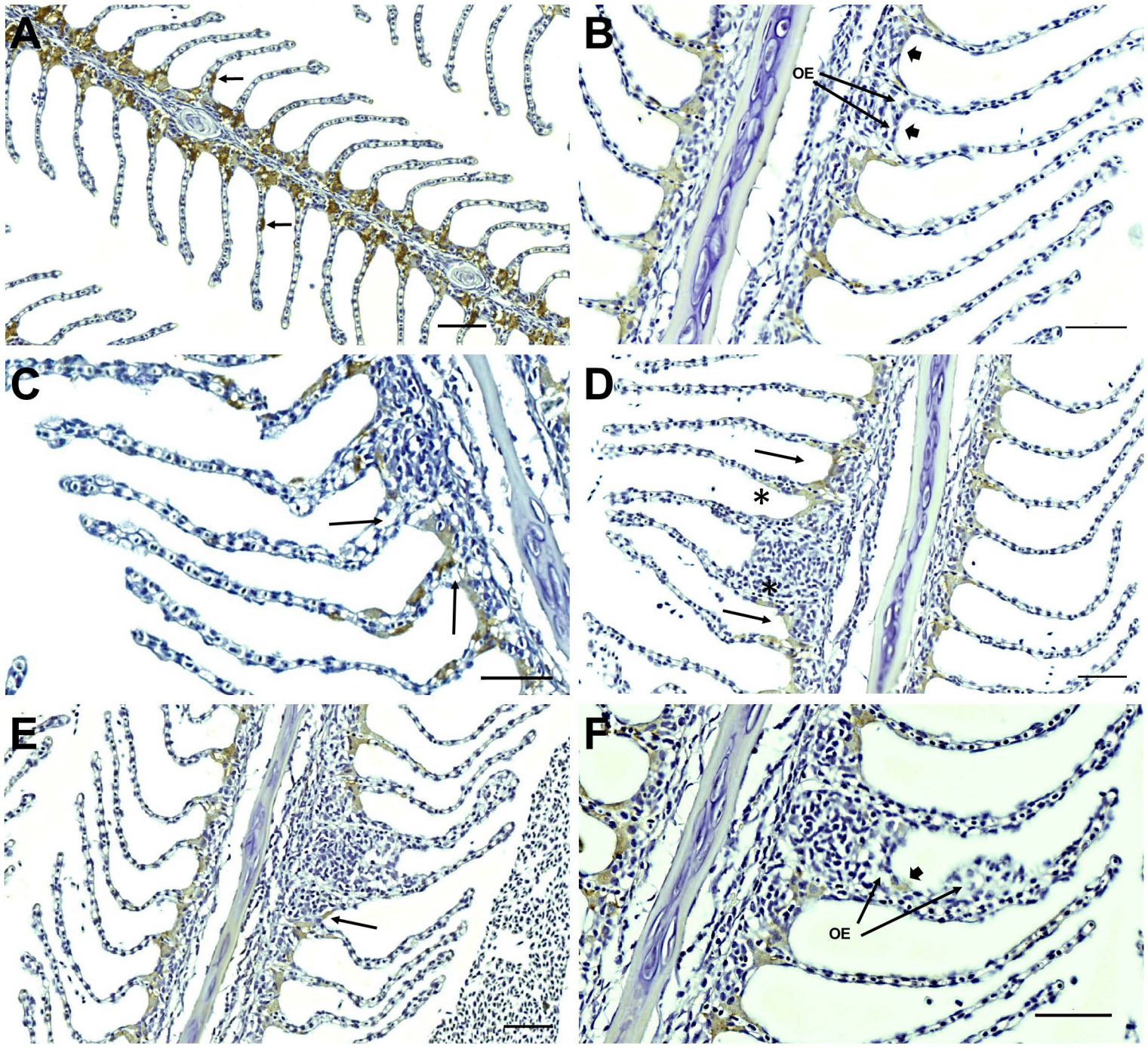
A
B
OE
C
D
*
*
E
F
OE

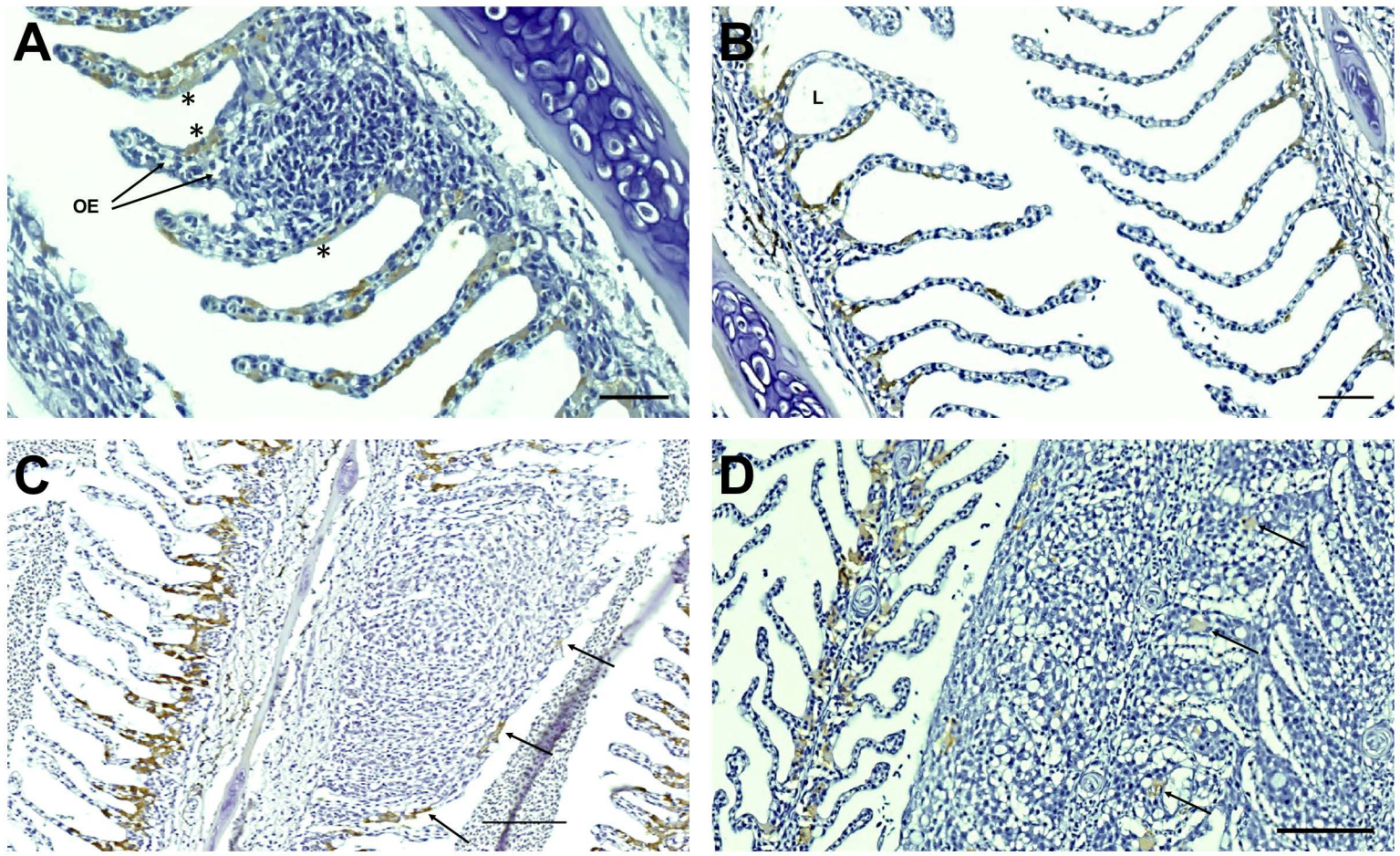
A
*
*
OE
*
B
L
C
D

OE

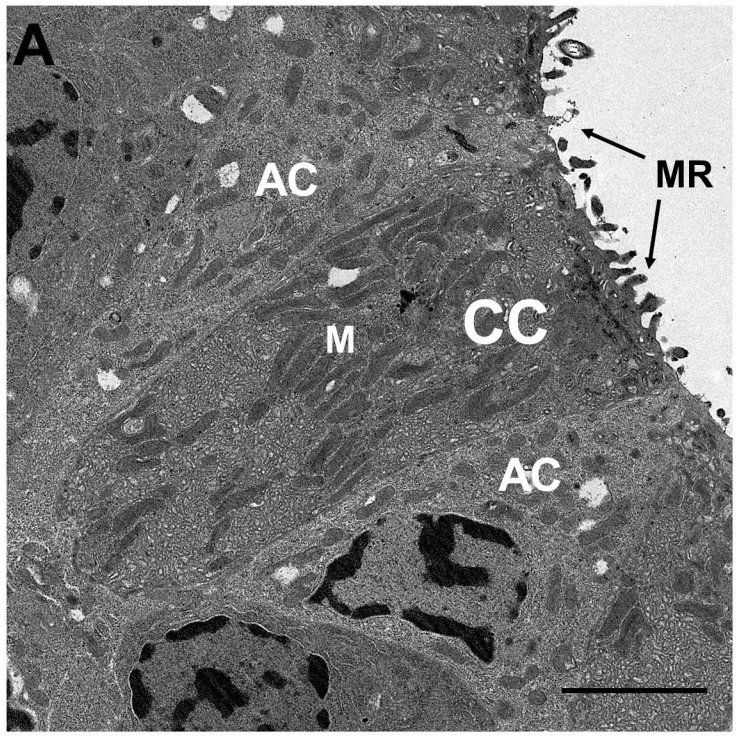

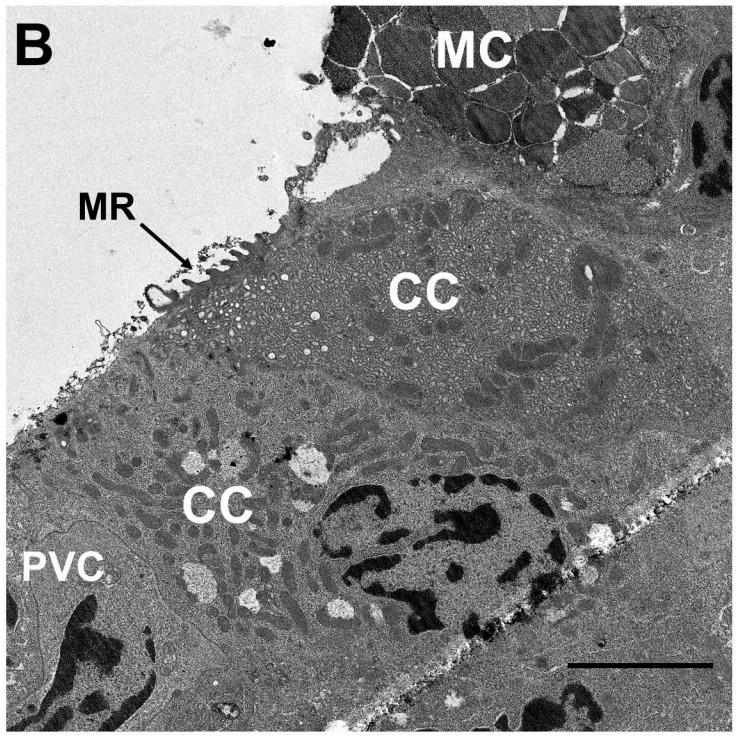

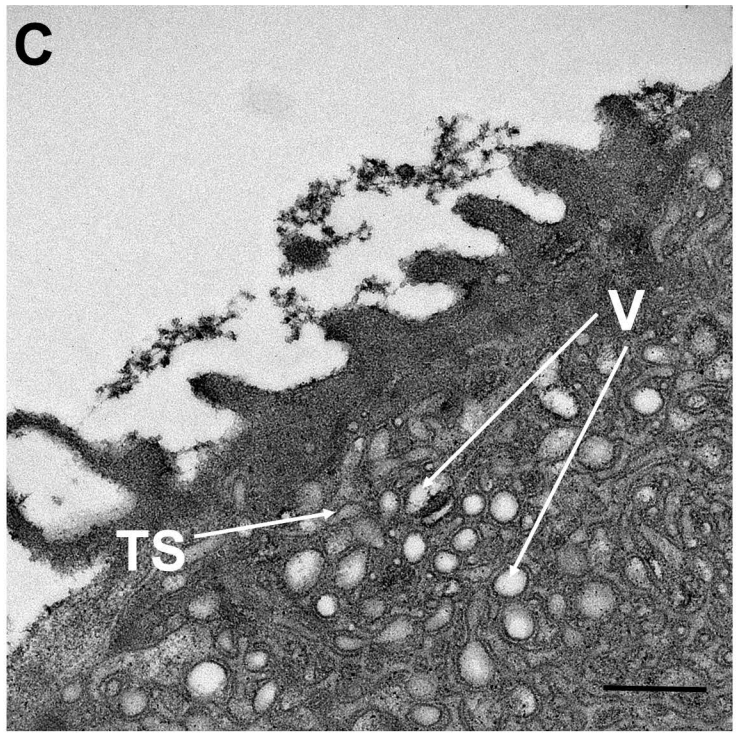

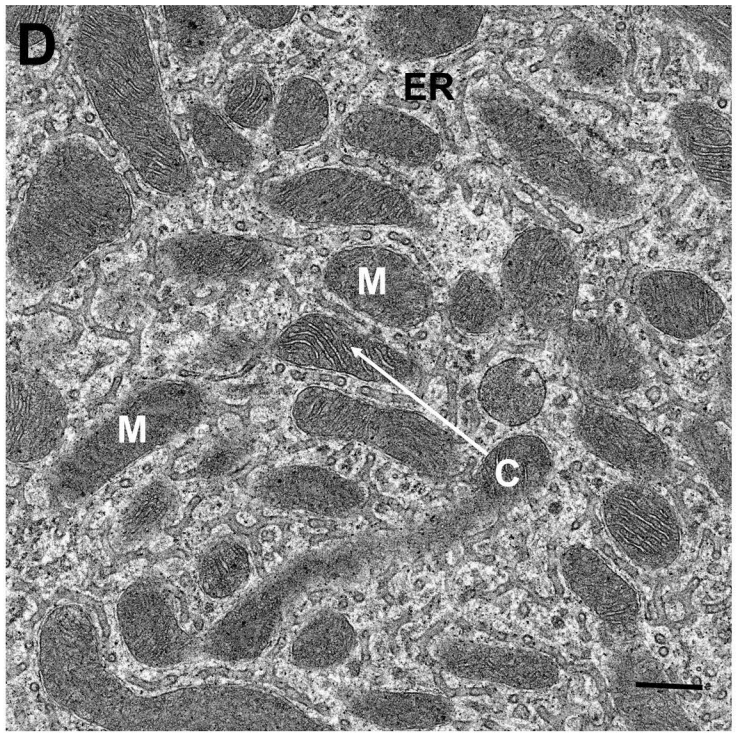

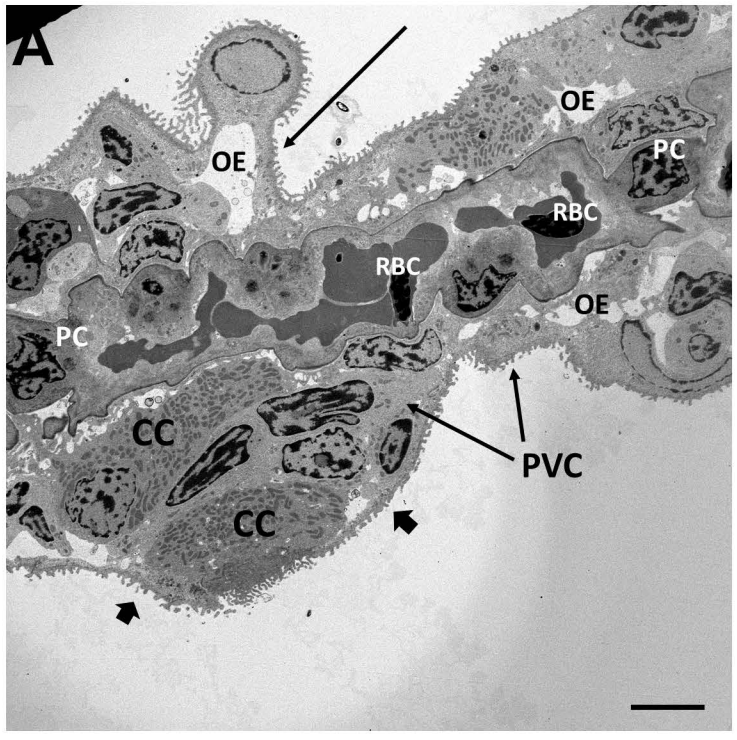
A
OE
OE
PC
RBC
RBC
OE
PC
CC
CC
PVC

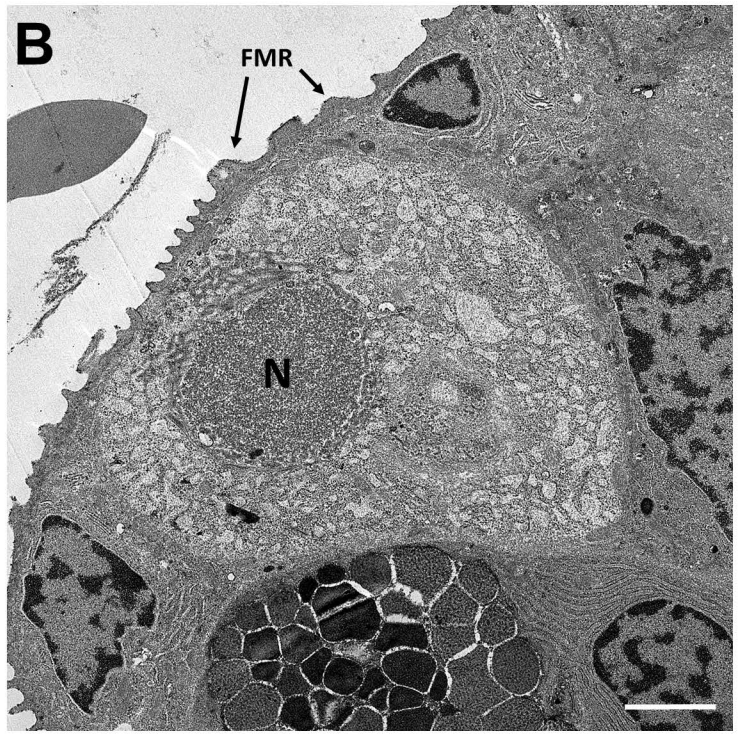
B
FMR
N

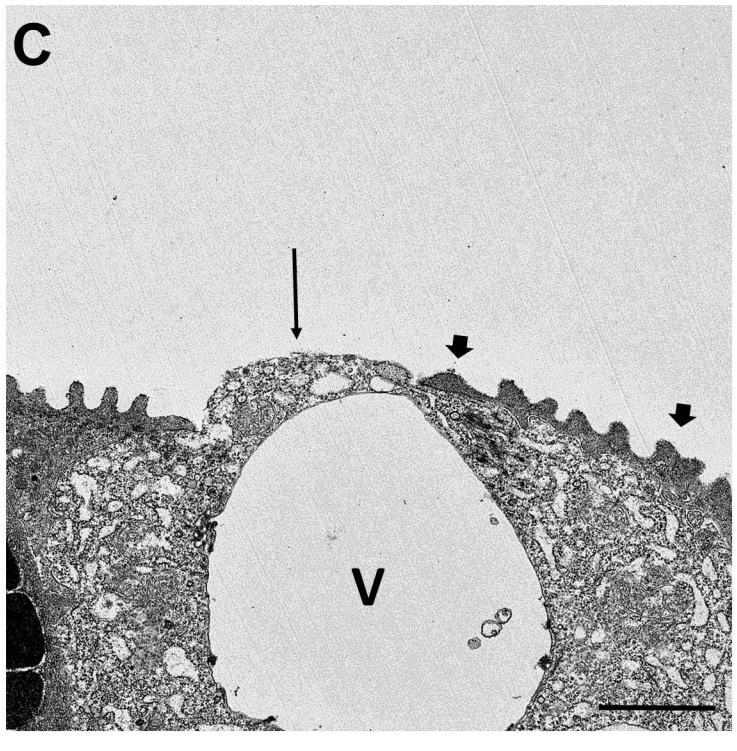
C
V

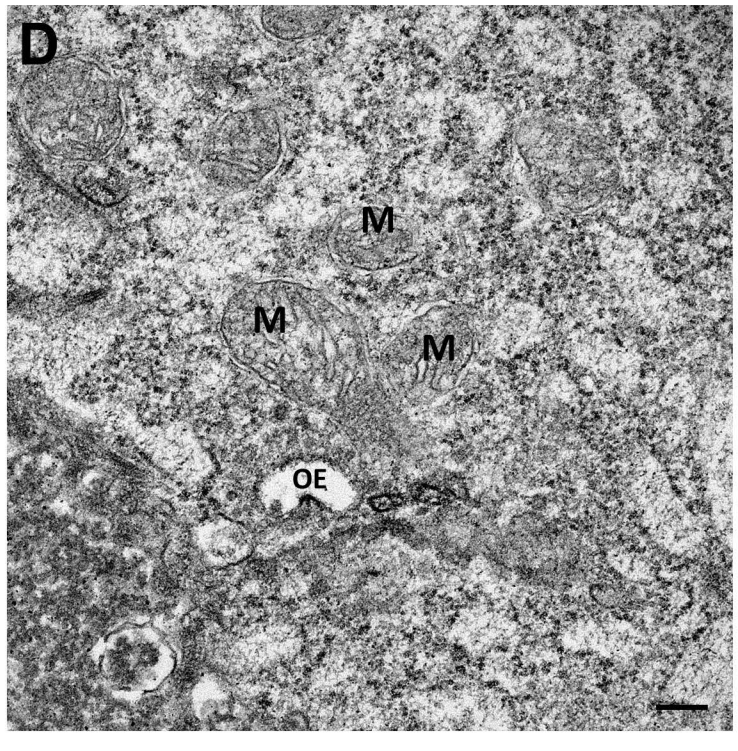
D
M
M
M
OE

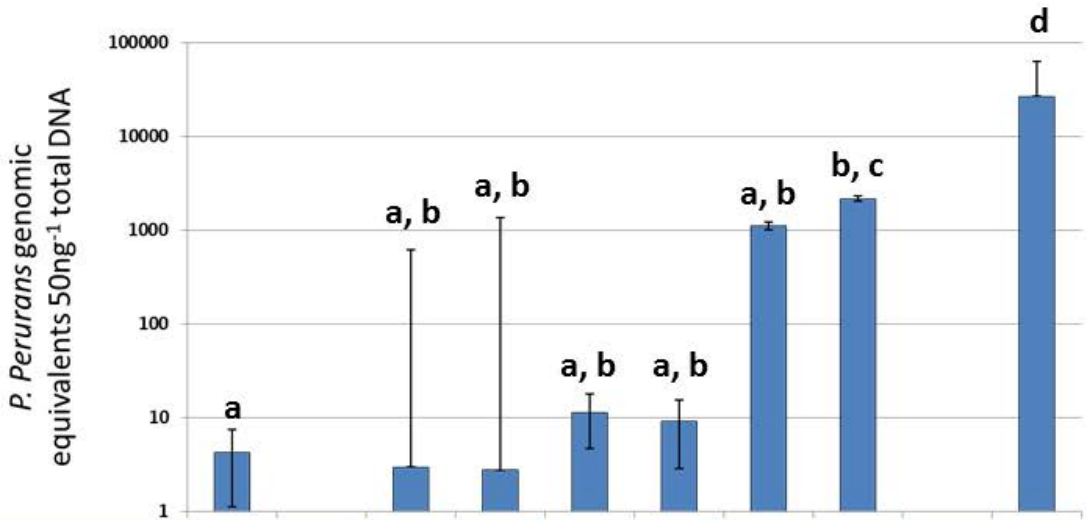

Group	A	B		C		D		E
Gill score	0	0-0.5		0.5-1		1-1.5		3.5-4.5
Sample type	-	L	N	L	N	L	N	L

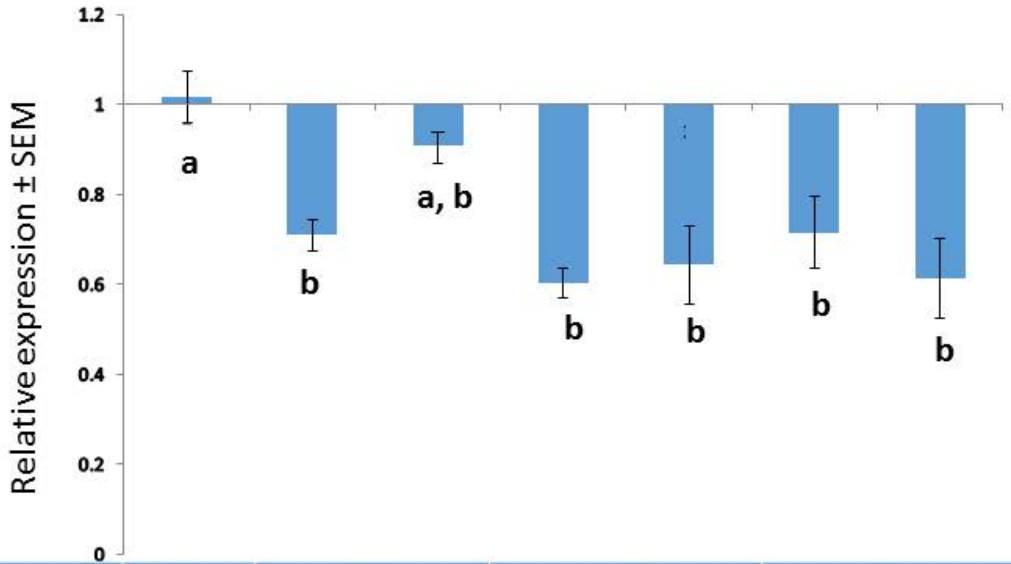

Group	A	B	C	D
Gill score	0	0-0.5	0.5-1	1-1.5
Sample type	-	L N	L N	L N